

# How Late can the Dark Matter form in our universe?

Abir Sarkar,<sup>1,2</sup> Subinoy Das,<sup>3</sup> Shiv.K.Sethi<sup>1</sup>

<sup>1</sup>Raman Research Institute  
Bangalore, India

<sup>2</sup>Indian Institute of Science  
Bangalore,India

<sup>3</sup>Indian Institute of Astrophysics  
Bangalore,India

E-mail: [abir@rri.res.in](mailto:abir@rri.res.in), [abir@physics.iisc.ernet.in](mailto:abir@physics.iisc.ernet.in), [subinoy@iiap.res.in](mailto:subinoy@iiap.res.in), [sethi@rri.res.in](mailto:sethi@rri.res.in)

**Abstract.** We put constraints on the epoch of dark matter formation for a class of non-WIMP (Weakly Interacting Massive Particle) dark matter candidates. These models allow a fraction of Cold Dark Matter (CDM) to be formed between the epoch of Big Bang Nucleosynthesis (BBN) and the matter radiation equality. We show that for such models the matter power spectra might get strong suppression even on scales that could be probed by linear perturbation theory at low redshifts. Unlike the case of Warm Dark Matter (WDM), where the mass of the dark matter particle controls the suppression scale, in Late Forming Dark Matter (LFDM) scenario, it is the redshift of the dark matter formation which determines the form of the matter power spectra. We use the Sloan Digital Sky Survey (SDSS) galaxy clustering data and the linear matter power spectrum reconstructed from the Lyman- $\alpha$  data to find the latest epoch of the dark matter formation in our universe. If all the observed dark matter is late forming, we find lower bounds on the redshift of dark matter formation  $z_f > 1.08 \times 10^5$  at 99.73 % C.L from the SDSS data and  $z_f > 9 \times 10^5$ , at the same C.L, from the Lyman- $\alpha$  data. If only a fraction of the dark matter is late forming then we find tentative evidence of the presence of LFDM from the Lyman- $\alpha$  data. Upcoming data from SDSS-III/BOSS (Baryon Oscillation Spectroscopic Survey) will allow us to explore this issue in more detail.

---

## Contents

<b>1</b>	<b>Introduction</b>	<b>1</b>
<b>2</b>	<b>Theory and motivation for Late Forming Dark Matter</b>	<b>2</b>
2.1	Models of LFDM	2
2.1.1	Scalar LFDM	3
2.1.2	Fermionic LFDM	3
<b>3</b>	<b>Cosmology of LFDM</b>	<b>4</b>
3.1	Modification in CAMB	4
<b>4</b>	<b>The Data</b>	<b>6</b>
<b>5</b>	<b>Data Analysis and Results</b>	<b>8</b>
<b>6</b>	<b>Discussion</b>	<b>11</b>
<b>7</b>	<b>Acknowledgment</b>	<b>13</b>

---

## 1 Introduction

In spite of extensive search, the particle nature of the dark matter (DM) is still a mystery. Until now, all the evidence for the dark matter has been obtained purely through its gravitational effects. Many observations such as Cosmic Microwave Background (CMBR) anisotropies [1–3], cosmological weak gravitational lensing [4], galaxy rotation curves [5], x-ray [6] and large scale structure survey (e.g. [7, 8]), etc., which span different length scales and epochs of the universe, have all confirmed the presence of dark matter but do not throw much light on its fundamental nature. That is why, most of the search for the particle constituent of the dark matter have been driven by aesthetic reason. One such dark matter candidate is Weakly Interacting Massive Particles (WIMP). The “WIMP miracle”, which has driven most of the direct and indirect experimental searches, relies on the coincidence between weak scale cross-section and the dark matter freeze-out cross-section needed to produce correct relic density. Unfortunately, all the direct [9–13], indirect [14–22] and collider [23, 24] searches for electroweak WIMP have not only produced null results but also different search results are in conflict with each other [25]. These anomalies definitely point to much richer physics in dark matter sector and might direct us to think out of the box—in other words to look for different physics and energy scale of dark matter beyond weak scale and super-symmetric candidates.

Once one encompasses non-WIMP candidates, the mass window for the dark matter opens up by many orders of magnitudes. If dark matter is produced through thermal processes which is the case for most of the fermionic dark matter models, it can be as heavy as TeV (super-WIMP [26]) or as low as keV (WDM) [27–29]. The lower bound arises from the so called Tremaine–Gunn bound [30] which arises from the conserved phase space density of the dark matter particle and its comparison with the densest packing of dark matter in the dark matter rich dwarf-spheroidal galaxy. But a scalar particle can also behave as dark matter. Either it can be a heavy scalar boson of GeV mass [31, 32] or it can be ultra-light axion or axion-like particle [33, 34] of sub-eV mass. For the case of such low mass bosons, a zero momentum condensate of scalar particle which arises due to coherent oscillation in a quadratic potential, behaves exactly as cold dark matter.

In this work, we are interested in epoch of dark matter formation rather than the mass of the DM particle. Here we ask the question: how late can a dark matter particle form in our universe. Unlike the case of electroweak WIMP where dark matter formed at very early epoch  $T \simeq \text{GeV}$ , there are models of dark matter, where the production can take place even after the BBN. These models belong to the category of “Late Forming Dark Matter” (LFDM) [35] where generally a late phase transition

is associated with dark matter production. The LFDM models are not only viable candidates of theoretically motivated non-standard dark matter they also have the potential to solve some long standing cosmological issues with the cold dark matter (CDM). For instance, it is a well known problem that N-body simulations based on CDM produce more galactic substructures (satellites) than observed [36, 37]. Also,  $\Lambda$ CDM is subject to “*too big to fail*” [38, 39] problem where the mass of sub-halo is too large in the milky way. One of the natural predictions of LFDM models is the suppression of power at small scale and therefore the LFDM scenario can potentially alleviate these issues with CDM.

In this work we consider a general class of LFDM model, where a radiation-like component gets converted into a cold dark matter state due to a late phase transition. We compare the results of our theoretical predictions with the SDSS galaxy clustering data and the linear matter power spectrum extracted from the Lyman- $\alpha$  data. One of the most important parameter in the theory is the redshift of dark matter formation which directly controls the suppression scale in the linear matter power spectra. The plan of the paper is as follows: in section 2, we briefly review the process of dark matter formation for a few well-motivated LFDM models. In section 3, we discuss the cosmology of LFDM and in section 4 we confront theoretical predictions with cosmological data. We present our result in sec 5 and present a summary of our results and possible future directions in section 6.

## 2 Theory and motivation for Late Forming Dark Matter

In this section we discuss how LFDM models differ with respect to their production mechanism and the formation epoch as compared to the other dark matter candidates. For the case of electroweak WIMP, the dark matter is formed through freeze-out when the temperature of the universe falls to  $m_{\text{DM}}/T \simeq 20$ —so the production happened at very early times ( $T \simeq$  a few GeV) much before the epoch of BBN. For the case of keV sterile neutrino WDM, when it is produced through active-sterile oscillation, the production epoch is  $T_{\text{pro}} \simeq 150$  MeV. For the case of axion dark matter, the scalar starts its coherent oscillation when the mass of the scalar field becomes of the order of Hubble parameter  $m_\phi \sim H(T)$ . For the accepted mass scale of sub-eV axion  $m_a \simeq 10^{-5}$  eV, the production happens at the QCD scale  $T \simeq 100$  MeV which also precedes the epoch of BBN.

The main difference between the models discussed above and LFDM models is that the formation of CDM can be as late as epoch corresponding to  $T \simeq$  eV. It is instructive to note that for warm dark matter (WDM) models, one gets suppression in matter power owing to the free streaming effects which are governed by the dark matter mass. But in our case, the suppression is controlled by the redshift of LFDM formation rather than its mass scale. This is the reason that in LFDM models the existing cosmological data directly constrains the redshift of dark matter formation.

### 2.1 Models of LFDM

There are many models of LFDM where the dark matter is created prior to recombination but after the epoch of BBN. One such model is when dark matter is produced from out of equilibrium decay of a long-lived charged particle [40] prior to recombination. Before the decay the charged particle was coupled to baryon-photon plasma and then decays to neutral dark matter particle which is only gravitationally coupled to baryons and photons.

Though in most of the models, linear matter power spectra gets a similar suppression at small scales, in this work, we will focus on a specific class of late forming DM, where an excess radiation component  $\Delta N_{\text{eff}}$  makes a phase transition to a dark matter state. We refer to the work [35] for details of the dark matter production mechanism as well as procedure for getting linear matter power spectra for LFDM theories where a scalar field starts coherent oscillation after phase transition and behaves like CDM. There is another way for the case of fermions where a neutrino like light dark fermions can also be trapped in small dark matter nuggets (section 3 of [41]) and starts behaving like CDM. In general, in these theories, one gets a higher  $N_{\text{eff}}$  compared to the case for standard  $\Lambda$ CDM cosmology. But we will also see that a tiny fractional increase in  $N_{\text{eff}}$  will suffice for producing correct

amount of CDM density if the dark matter is formed a few e-folding before the matter radiation equality. The recent constraints on  $N_{\text{eff}}$  from Planck and WMAP prefer the existence of a fractional dark radiation  $N_{\text{eff}} = 3.62_{-0.48}^{+0.50}$  at 95 percent C.L. [42]. Thus this model is in complete agreement with the cosmic microwave background measurements. In fact, if one starts with a fully thermalised dark radiation-like component and a fraction of it turns into CDM, it might leave a fractional dark radiation (equivalent to partially thermalised light eV sterile neutrino) at the epoch of CMB which might even be preferred by data [43].

In this work we consider two cases: (a) scalar and (b) fermionic LFDM for our numerical work. Both of them are triggered by a late phase transition and the epoch of phase transition  $z_f$  remains the main parameter to be constrained in both the cases. Below we present a brief review of these two cases of LFDM.

### 2.1.1 Scalar LFDM

A dynamical scalar field with a potential  $V(\phi)$  can be held in a metastable minimum by thermal effects until a critical temperature is reached [35]. After the universe cools down below the critical temperature, the scalar is released to oscillate around the minimum of a quadratic potential and starts behaving like CDM with equation of state  $w = 0$ . As discussed in [35] it is possible to achieve it by interactions beyond the standard model in the neutrino sector; these interactions allow the the scalar field to be held in a metastable minimum. Once the neutrino temperature drops below a critical value, the LFDM is formed. One of the advantage of the LFDM appearing from neutrino dark energy theories is that the epoch of phase transition is naturally predicted to be very late and is subjected to constraints arising from linear perturbation theory. The range for LFDM formation epoch arising from neutrino dark energy is given by [35]:  $1\text{eV} < T_f < 10^3\text{eV}$ . The length scales corresponding to the horizon entry for this range of epochs are:  $2 \times 10^{-2} h Mpc^{-1} < k_f < 20 h Mpc^{-1}$ . This bound is purely theoretical assuming natural values of the coupling constants.

As discussed above, even though QCD axion can not be late forming DM, there are ultra light axion-like particles,  $m \sim 10^{-20}\text{eV} - 10^{-22}\text{eV}$ , arising from string theory that can behave as LFDM depending on their masses [44–46]. In these cases, the linear matter power spectra has similar suppression as the LFDM, appearing in the context of neutrino dark energy. It is interesting to note that in recent work [47] a CDM-like particle interacting with neutrino or dark radiation can also produce a LFDM-like power spectra with damped oscillation. But in that case the dark matter is present from a very early epoch unlike the case we are interested in.

### 2.1.2 Fermionic LFDM

A light fermion-like eV sterile neutrino can be trapped into a fermion nuggets by a phase transition driven by a strong scalar interaction. Initially the idea of fermion nugget formation was proposed in [48]. But in their work, the dark matter like nuggets form much later than matter-radiation equality. In a recent work (section 3 of [41]), it was shown that light sterile fermion behaving like dark radiation can be trapped in heavy dark matter nuggets. The stability of the nugget is achieved when attractive fifth force is balanced by degenerate Fermi pressure of the light fermions inside the nuggets. There are mainly two main equations which need to be solved to get the nugget mass, radius and density:

$$\phi'' + \frac{2}{r}\phi' = \frac{dV(\phi)}{d\phi} - \frac{d[\ln(m(\phi))]}{d\phi} T_{\mu}^{\mu} \quad (2.1)$$

$$\frac{dp}{d\phi} = \frac{d[\ln(m(\phi))]}{d\phi} (3p - \rho) \quad (2.2)$$

We refer to [49] for detailed derivation of these equation. Briefly, the first one is the Klein Gordon equation for  $\phi(r)$  under the potential  $V(\phi) = \lambda\phi^4$  where the fermions act as a source term for  $\phi(r)$ . The other equation tells us how the attractive fifth force is balanced by local Fermi pressure. The details of dark matter nugget formation with exact numerical solution and particle physics model will be reported soon in a different work [50].

Once the phase transition happens, there is a fractional drop in neutrino degrees of freedom  $N_{\text{eff}}$ , as the radiation component starts behaving as CDM immediately after the phase transition. This gives us one more parameter of interest:  $N_{\text{eff}}$ .

Since the epoch of phase transition until the present, LFDM redshifts as normal CDM, one gets

$$\rho_{\text{lfdm}}^{(z_f)} = \rho_{\text{lfdm}}^{(0)} (1 + z_f)^3 \quad (2.3)$$

Now assuming that a fraction of excess radiation component got converted into a fraction of CDM density,  $f_{\text{lfdm}}$ , at  $z = z_f$ , we get the decrement in the effective number of neutrino degrees of freedom,  $\Delta N_{\text{eff}}$  to be:

$$\Delta N_{\text{eff}} \rho_{\nu}^{(z_f)} = f_{\text{lfdm}} \rho_{\text{lfdm}}^{(0)} (1 + z_f)^3 \quad (2.4)$$

where  $\rho_{\nu}^{z_f}$  is the energy density of one neutrino-like radiation species at the formation redshift. This yields:

$$\Delta N_{\text{eff}} = f_{\text{lfdm}} \frac{\rho_{\text{cdm}}^{(0)}}{\rho_{\nu}^{(0)}} = 1.7 f_{\text{lfdm}} \Omega_{\text{CDM}} h^2 \left( \frac{10^5}{1 + z_f} \right) \quad (2.5)$$

It should be noted that  $\Delta N_{\text{eff}}$  is inversely proportional to the redshift of formation. As the effective number of neutrino degrees of freedom dynamically change in this model, observational constraints on  $N_{\text{eff}}$  from different observations need to be interpreted properly.

For instance, for  $z_f < 10^{10}$ , the BBN constraints, which depend on the in situ value of  $N_{\text{eff}}$  during the era of BBN, apply to the value of  $N_{\text{eff}}$  before the epoch of dark matter formation. [51–53]. On the other hand, CMBR and galaxy clustering data, which are influenced by the history of changes in  $N_{\text{eff}}$ , are also sensitive to the final  $N_{\text{eff}}$ . Throughout this paper  $N_{\text{eff}}$  corresponds to the initial degrees of freedom. We also note that, for most of the range of  $z_f$  of interest,  $\Delta N_{\text{eff}}$  is generally smaller than the current precision on  $N_{\text{eff}}$  from different data sets; for instance, it follows from Eq. (2.5) that even if  $f_{\text{lfdm}} = 1$ ,  $\Delta N_{\text{eff}} = 0.2$  for  $z_f = 10^5$ , assuming the best fit Planck parameters for  $\Omega_{\text{CDM}} h^2$ . As noted above we also consider the case when the LFDM contributes only a fraction to the observed CDM at the present and this fraction is denoted by  $f_{\text{lfdm}}$ .

It is instructive to note that in both the above cases, once  $z_f$  is fixed, the power spectra is almost uniquely determined as the model has to match the correct dark matter relic density. This also means that the resulting constraint on  $z_f$  from the data would be valid for both the fermionic and scalar cases of LFDM.

### 3 Cosmology of LFDM

There are mainly two main features of LFDM cosmology that manifest themselves in the matter power spectra. First, there is a sharp break in the power at the co-moving scale  $k = aH_e$ ; here  $H_e$  is the Hubble scale at the epoch of phase transition. Second, there are damped oscillations at smaller scales. Both of these can be seen in Figure 1, in which we show the transfer function for massless neutrinos. Before the phase transition, due to strong coupling of the scalar with neutrinos, the scalar perturbations follow neutrino perturbations. We compute the the density perturbations of the massless neutrinos at  $z = z_f$  and match that to the initial conditions of the CDM component at that epoch.

#### 3.1 Modification in CAMB

It is interesting to note that even though the physics of scalar and fermionic LFDM production can be quite different, the initial condition of the LFDM at the formation epoch can be taken from the a neutrino-like component at the epoch corresponding to  $z = z_f$ . This is because in both the cases, the density perturbation of a neutrino or a dark radiation component provides the initial density fluctuation of LFDM at the production epoch  $z_f$ . The evolution of neutrino density perturbation is

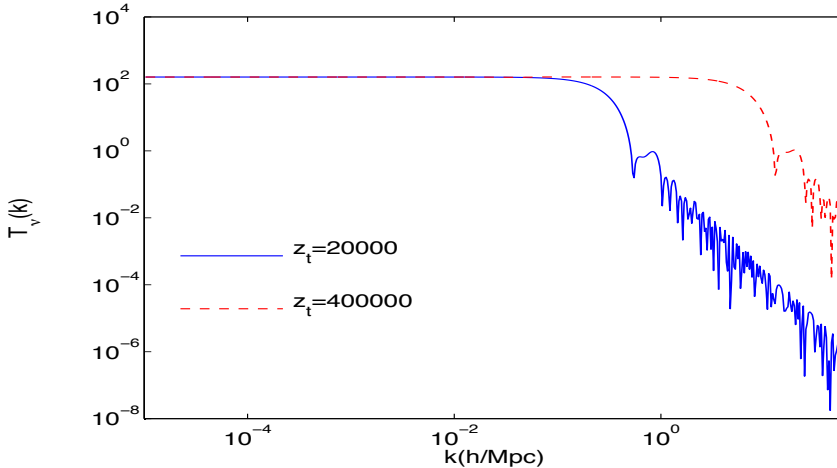


**Figure 1.** The unnormalized transfer functions for the neutrino density perturbation  $\delta_\nu$  at two different epochs of LFDM formation are shown. This fluctuation provides the initial condition for the LFDM which evolves like cold dark matter from  $z_f$  until present epoch.

obtained by solving a series of coupled differential equations [54] involving Legendre Polynomials

$$\begin{aligned}
 \dot{\delta} &= -\frac{4}{3}\theta - \frac{2}{3}\dot{h} \\
 \dot{\theta} &= k^2 \left( \frac{\delta}{4} - \sigma \right) \\
 2\dot{\sigma} &= \frac{8}{15}\theta - \frac{3}{15}kF_3 + \frac{4}{15}\dot{h} + \frac{8}{5}\dot{\eta} \\
 \dot{F}_l &= \frac{k}{2l+1} (lF_{l-1} - (l+1)F_{l+1})
 \end{aligned} \tag{3.1}$$

The solution for  $\delta_\nu$  is an exponentially damped oscillation at sub-horizon scales [54]. Physically, it represents the free-streaming effects of highly relativistic neutrinos. In Figure 1, we plot transfer function for standard model neutrino density fluctuation by solving the above equations using the publicly available code `CAMB`[55] for two different values of  $z_f$ . Our main modification in `CAMB` is to evolve it up to a redshift  $z_f$  without CDM and extract the transfer function for neutrino perturbation at  $z = z_f$ ,  $\delta_\nu(z_f)$ , and use that for the LFDM initial condition for density fluctuation at the epoch of its formation. We then evolve LFDM perturbation just like CDM to get the power spectra at the present epoch. So the oscillations at small scales in the final power spectra at  $z = 0$  is a signature of

the fact that LFDM obtained its initial density fluctuation from neutrino perturbation at  $z_f$  which was damped and oscillatory at scales smaller than the horizon size of the Universe at  $z = z_f$ .

The main goal of our work is to find out how late the dark matter can form, i.e, to find out the minimum value of the formation redshift  $z_f$ . As discussed in the previous section, the formation of dark matter happens via the transition of the scalar field. We are therefore able to formulate the cosmological impact of LFDM in terms of three parameters: the initial relativistic neutrino degrees of freedom:  $N_{\text{eff}}$ , the epoch of the formation of CDM:  $z_f$ , and the fraction of CDM that forms at  $z = z_f$ :  $f_{\text{lfdm}}$ .

A set of power spectra with different  $z_f$  and  $N_{\text{eff}}$  are shown in Figure 2. In each case we have plotted the usual  $\Lambda$ CDM power spectrum for comparison.

As Figure 2 shows, the new features introduced by LFDM are largely determined by the variation of  $z_f$ . The scale imprinted on the matter power spectrum is determined by the scale of horizon entry at  $z = z_f$ ,  $k_e$ . For the horizon entry in the radiation dominated era:

$$k_e = \frac{H_0}{c}(1 + z_f)\Omega_\gamma(1 + 0.227N_{\text{eff}}) \quad (3.2)$$

Here  $\Omega_\gamma$  is the radiation contribution from photons. The matter power spectrum is suppressed at scales below the corresponding scale for  $k_e$ . This suppression can be understood as follows: the LFDM obtains its initial conditions from massless neutrinos. On the super horizon scales, the massless neutrinos behave like other forms of matter such as the CDM (for details see e.g. [54, 56]). However, unlike CDM, the perturbations in this component are washed out owing to free-streaming on scales smaller than horizon size. As  $z_f$  is increased the feature shifts to larger  $k_e$ , or smaller scales. As  $z_f$  tends to infinity, the LFDM matter spectrum approaches the  $\Lambda$ CDM results. This also motivates our choice of the cosmological data for constraining the LFDM model.

## 4 The Data

As discussed above, we can theoretically analyze the impact of the late forming dark matter in terms of three parameters:  $z_f$ ,  $f_{\text{lfdm}}$  and  $N_{\text{eff}}$ . For a given  $z_f$  and  $f_{\text{lfdm}}$ ,  $\Delta N_{\text{eff}}$  can be expressed in terms of these parameters for a given  $\Omega_{\text{DM}}h^2$  (Eq. (2.5)), which we assume to be fixed and given by the best-fit Planck estimate for the six-parameter spatially-flat  $\Lambda$ CDM model [1].

The two parameters— $z_f$  and  $N_{\text{eff}}$ —affect the linear power spectrum at different scales. The main impact of changing  $N_{\text{eff}}$  is to alter the matter radiation equality epoch. This shifts the peak of the matter power spectrum. As the SDSS data on the galaxy power spectrum gives the power at such scales:  $k=0.02\text{--}0.1\text{ h/Mpc}$ , this data is sensitive to the variation of  $N_{\text{eff}}$ . We use the SDSS DR7 release data [57]. For  $k > 0.1$ , the SDSS data cannot be directly compared to the predictions of linear theory as non-linearities set in for such scales. We use the HALOFIT model embedded in CAMB to obtain the non-linear power spectrum for comparison with the SDSS galaxy power spectrum; this procedure allows us to use the data for  $k \lesssim 0.2$ . It is instructive to note that though the HALOFIT works mainly for  $\Lambda$ CDM and might not work for other dark energy models of constant equation of state differing from  $w = -1$  [58], in LFDM cosmology, the background evolution is exactly same as the  $\Lambda$ CDM model after the phase transition has occurred deep in radiation dominated era. So we expect HALOFIT to be a good approximation for mildly non-linear power spectra for comparison with SDSS galaxy power spectrum.

As seen in Figures 1 and 2 above, the main effect of late formation redshifts  $z_f$  is to suppress the power at scales  $k > 0.1\text{ h/Mpc}$ . Such scales are not directly accessible from the data on galaxy power spectrum at low redshifts. It is known that Lyman- $\alpha$  clouds observable at intermediate redshifts ( $2 < z < 5$ ) probe mild over densities ( $\delta \simeq 10$ ) of the density field. The data from Lyman- $\alpha$  clouds can be used to reconstruct the linear matter power spectrum for scales comparable to the Jeans' scale of the intergalactic medium in the relevant redshift range [59, 60]. Here we use the data in the range:  $0.2 < k < 4.8\text{ h/Mpc}$  from [59, 61]. From Figure 1 and 2, it is clear that the scales probed by the Lyman- $\alpha$  data are far more sensitive to the variation in  $z_f$ . As  $z_f$  is increased the oscillations seen in

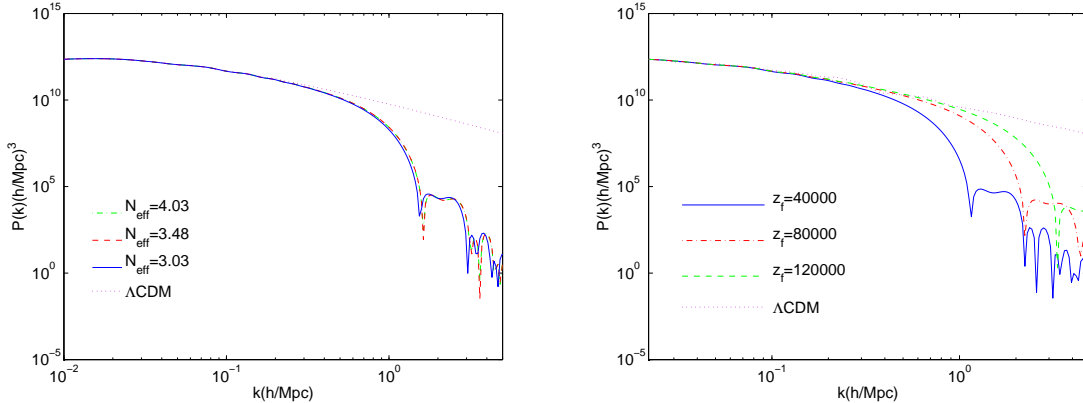


**Figure 2.** The LFDM power spectra (unnormalized) are shown for a range of formation redshift  $z_f$  and relativistic neutrino degrees of freedom. The left panel shows the impact of changing  $N_{\text{eff}}$  for a fixed  $z_f = 52000$ . In the right panel, LFDM power spectra are shown for different  $z_f$  for  $N_{\text{eff}} = 3.04$ .

the power spectra move to larger values of  $k$  (or smaller scales) with the power spectrum approaching the  $\Lambda$ CDM model as  $z_f$  tends to very large values.

Other data sets at scales overlapping with SDSS data are available, e.g. WiggleZ survey [62] with scale coverage  $0.01 < k < 0.5 \text{ h Mpc}^{-1}$ . We could obtain supplementary information from WiggleZ data but it doesn't expand the range of scale we already consider. Or the two data sets we use allow us to obtain the tightest possible constraints on LFDM models within the framework of linear (and mildly non-linear) theory. Cosmological weak lensing provides a powerful probe of the matter power spectrum (e.g. [63]). We do not use it here because the scales probed by the cosmological lensing are larger than the those probed by the Lyman- $\alpha$  data (e.g. [61]) so we cannot use it to get better constraints on the formation redshift  $z_f$ . Also in this paper we only consider the available data on measured or reconstructed power spectra. The reconstructed power spectrum is not readily available in the literature (e.g. [63]). This means we have to compute the observables presented in the literature from LFDM power spectra. We shall undertake this task in future works.

Our choice of Lyman- $\alpha$  data is also governed by the availability of reconstructed linear power spectra. In all the available data on the linear matter power spectrum, the data we use provides a probe of the smallest scales. It is based on the high spectral resolution QSO spectra (total of 53 QSOs including 30 observed at high spectral resolution [59]). This one-dimensional data allows reconstruction of the linear 3-dimensional matter spectrum. However the low-resolution SDSS data, which is available for a much larger number of QSOs, doesn't allow this reconstruction (for details and discussion see e.g. [59, 64]). This means that a comparison with the ongoing survey SDSS-III/BOSS, which will finally obtain spectra of 160000 QSOs in the redshift range  $2 < z < 7.5$  [65], will require

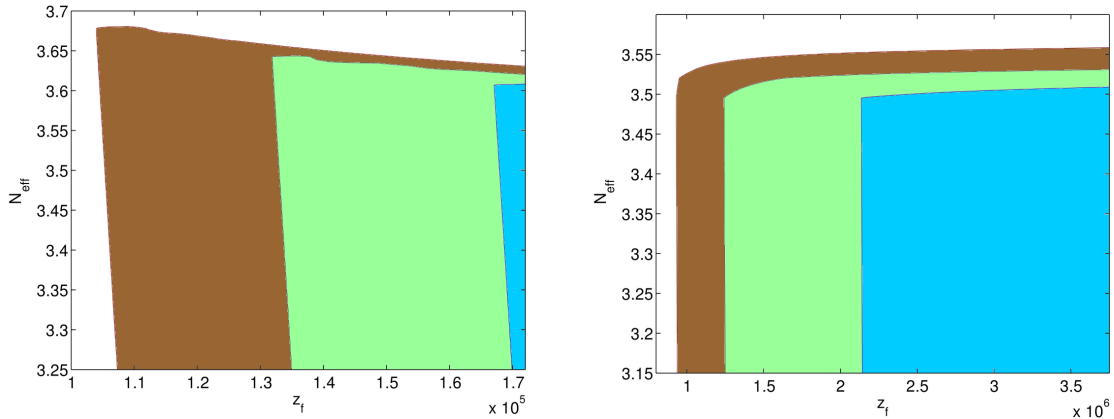


**Figure 3.** The allowed regions in the  $z_f$ - $N_{\text{eff}}$  plane are shown from the power spectra of SDSS (Left Panel) and Lyman- $\alpha$  (Right Panel) data. In each Panel, the blue, green and the brown regions indicate the 68%, 95.4% and 99.73% confidence levels, respectively.

us to simulate the Lyman- $\alpha$  spectra for our class of models. We consider it beyond the scope of this paper and plan to undertake this study in the near future. We also note that even the low spectral resolution Lyman- $\alpha$  could be a powerful probe of the matter power spectrum at small scales because of two reasons: (a) the measured 1-dimensional flux power spectrum by the Lyman- $\alpha$  data receives contribution from a wide range of scales of the 3-dimensional power spectrum, (b) the relation between the density field and the observable is non-linear (e.g. [66]).

## 5 Data Analysis and Results

The two data sets—SDSS galaxy power spectrum and the linear power spectrum reconstructed from the Lyman- $\alpha$  data—allow us to investigate the range of scale:  $k = 0.02$ – $5h/Mpc$ . However, these two data sets do not have the same bias with respect to the underlying density field, and therefore the overall normalization constant is different for the two cases. In other words, we can probe the shape of the power spectrum in the aforementioned range of scales and not its overall normalization. We consider four parameters for each data set:  $N_{\text{eff}}$ ,  $z_f$ ,  $f_{\text{fdm}}$ , and  $C$ , where  $C$  corresponds to an overall normalization which is marginalized. For our analysis we search the best-fit in the range:  $N_{\text{eff}} = 3$ – $4$ , which encompasses the current range of constraints on  $N_{\text{eff}}$  [52, 53].

As noted above we compute a suite of models for different  $z_f$  and  $N_{\text{eff}}$  by modifying CAMB. We extract unnormalized power spectra and the normalization is fixed by comparison with data. Model predictions for a range of  $f_{\text{fdm}}$  are obtained by assigning different weights to the initial conditions; for instance, for  $f_{\text{fdm}} = 1$ , the initial condition for the CDM component is drawn from massless neutrinos at  $z = z_f$ . For a smaller value of  $f_{\text{fdm}}$ , the initial conditions are a mix of the CDM component in the pre-transition phase and the massless neutrino. This also means that we need to vary only two parameters ( $z_f$  and  $N_{\text{eff}}$ ) in CAMB for obtaining the power spectra for all the four parameters. For likelihood analysis we have used the range of  $z_f$  to be 24000–180000 with an interval of  $\Delta z_f = 4000$  while analyzing the SDSS data and  $z_f = 62000$ – $4000000$  with an interval of  $\Delta z_f = 2000$  for the Lyman- $\alpha$  data. The range of the  $z_f$  is different for the two data-sets because the Lyman- $\alpha$  data covers much smaller scales as compared to the SDSS data. The smallest scale probed by the Lyman- $\alpha$  data,  $k \simeq 4Mpc^{-1}$  enters the horizon at  $z \simeq 4000000$  which is the highest  $z_f$  we have considered. Similarly,  $N_{\text{eff}}$  is also finely sampled to ensure convergence of the likelihood procedure.

We use 45 band-powers from the SDSS galaxy data and 12 points from the reconstructed linear power spectrum from the Lyman- $\alpha$  data. The best-fit  $\chi^2$  for the two case is 65 and 10.5, respectively.

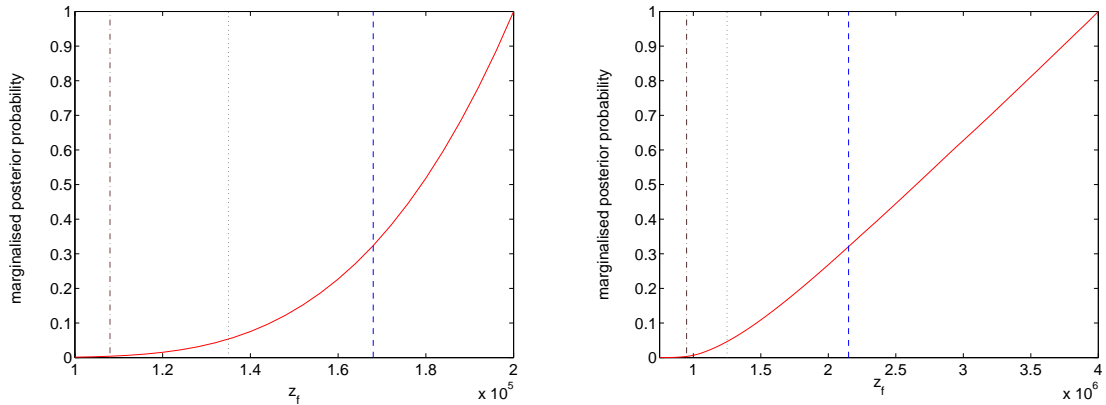


**Figure 4.** Marginalized posterior probability for  $z_f$  from SDSS data (Left Panel) and Lyman- $\alpha$  data (Right Panel) are shown. The dashed (blue), dotted (green) and dot-dashed (brown) lines indicate the 68%, 95.4% and 99.73% regions, respectively.

The multi-parameter contours and posterior probabilities are computed by marginalization, i.e. the integration of the likelihood function  $\exp(-\chi^2/2)$  over redundant parameters.

We first consider the case  $f_{\text{ldm}} = 1$ , or all the observed CDM at the present is formed at  $z_f$ . In Figure 3, we show the confidence limits for  $z_f$  and  $N_{\text{eff}}$  for the two data sets. Both the data sets result in a lower limit on the value of  $z_f$ . The Lyman- $\alpha$  data results in stronger constraints on  $z_f$ . This result follows from Eq. (2.5) and Figure 2 which show that an increase in  $z_f$  results in the feature in the power spectrum shifting to smaller scales. As Lyman- $\alpha$  data probe smaller scales, we expect a tighter constraint on  $z_f$  from these observations. We note that for both the data sets the floor on the value of  $\chi^2$  is set by the  $\Lambda$ CDM model. Or we do not find any evidence of an improvement over the  $\Lambda$ CDM model within the framework of a two-parameter LFDM model.

The marginalized posterior probabilities for  $z_f$  are shown in Figure 4. We note that the temperature of the universe corresponding to  $z = z_f$  from the two data sets is in the range 30–500 eV. These lower limits on the transition temperature are far below the constraints on production redshifts in the warm dark matter models; in such models a dark matter particle with mass  $m > 1$  keV is invoked [29] and the production redshift lies before the epoch of BBN at a temperature  $T \simeq$  MeV.

We next consider the case  $f_{\text{ldm}} < 1$ . Or only a fraction of the CDM observed at the present originated at  $z = z_f$ . This expands the parameter space under consideration and yields more interesting results. In Figure 5, we show  $z_f$ – $f_{\text{ldm}}$  contour plots after marginalizing over  $N_{\text{eff}}$  and the overall normalization  $C$ . The SDSS data gives results similar to the previous case with slightly looser bound on  $z_f$ . The Lyman- $\alpha$  data, on the other hand, results in very different outcome, as compared to the earlier case. The  $z_f$ – $f_{\text{ldm}}$  plain splits into two separate regions in this case. The region corresponding

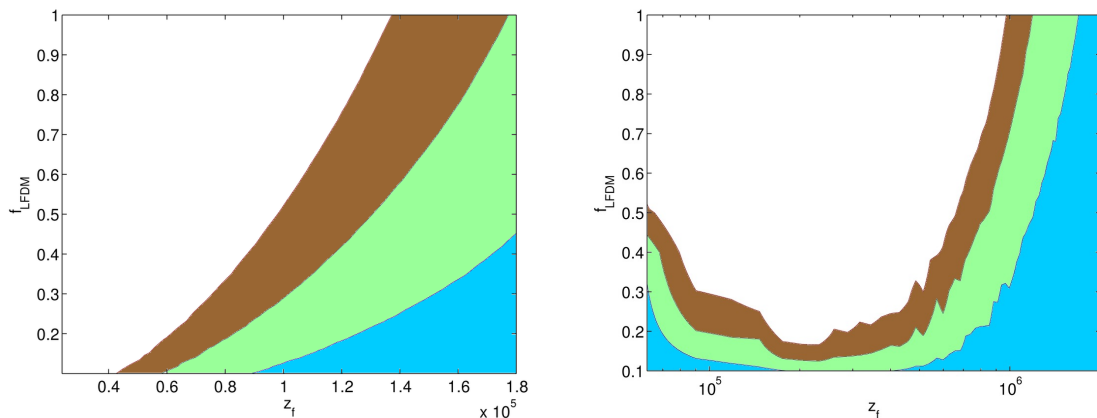


**Figure 5.** Contours of  $z_f$  and  $f_{\text{lfdm}}$  obtained using SDSS data (Left Panel) and the Lyman- $\alpha$  data (Right Panel).

to  $z_f < 10^5$  is ruled out by the SDSS data but is unconstrained by the Lyman- $\alpha$  data. This underlines the importance of using two data sets at different scales for our analysis. Larger values of  $z_f$  is allowed by both the data sets. Further, the Lyman- $\alpha$  data results in a better fit as compared to the  $\Lambda$ CDM case, as seen in Figure 6, for a large range of values of  $f_{\text{lfdm}}$  (this inference is nearly independent of  $N_{\text{eff}}$ ). In particular,  $f_{\text{lfdm}} = 0.1$  results in a better fit for the entire range of  $z_f$ . To understand this improvement of the fit, we show the Lyman- $\alpha$  data alongside many theoretical models in Figure 7. While  $\chi^2 \simeq 11$  for the  $\Lambda$ CDM models, it reduces to 3.5 for many models for  $f_{\text{lfdm}} = 0.1$ . This improvement is largely owing to the two data points for the largest  $k$ . This shows the importance of using the small scale data for unraveling the nature of LFDM models.

Our analysis clearly shows that LFDM models with a non-zero  $f_{\text{lfdm}}$  provide a better fit to the data. However, while significant, our results need further explanation. In our analysis we assume many cosmological parameters to be fixed to their Planck best-fit values. Within the framework of spatially-flat  $\Lambda$ CDM model, the relevant cosmological parameters— $\Omega_{\text{CDM}}h^2$ ,  $\Omega_B h^2$ ,  $h$ ,  $n_s$ —have been estimated at unprecedented precision [1]. For a given angular scale  $\ell$ , the CMBR anisotropies receive dominant contribution from three-dimensional scales  $k$  such that  $\ell \simeq k\eta_0$ ;  $\eta_0 = 13670 \text{ Mpc}$  for the best-fit Planck parameters. As Planck measures CMBR anisotropies for  $\ell < 2000$ , the smallest scale to make significant contribution to these observations is  $k \simeq 0.15 \text{ Mpc}^{-1}$ , which lie in the range of scales probed by SDSS; Planck results are compatible with the SDSS DR7 data we use in this paper (Figure 20 of [1]). However, these scales are larger than the scales involved in Lyman- $\alpha$  measurements and therefore the Lyman- $\alpha$  data gives us independent information of the matter power spectrum on scales not probed by Planck. This also means that we are justified in assuming priors on cosmological parameters from Planck, even though we still need to explore the whole range of parameters allowed by Planck to put our result on a firmer footing.

In Figure 8 we compare the predictions of our model with other models in which the power is suppressed at small scale with respect to the  $\Lambda$ CDM model. One such model is the WDM model; in Figure 8 we show the matter power spectrum for a much-studied WDM model [29]. In WDM models, the neutrino-like particle is much heavier than the usual standard model neutrino and its mass density is matched to the present day dark matter mass density. In such class of models, the WDM component can begin to cluster after it become non-relativistic at a time when  $T \lesssim m_{\text{WDM}}$ . However, owing to the fact that the WDM particle remains semi-relativistic for a long time after this era, the matter power is suppressed on a large range of scales that enter the horizon during this period (for details see e.g. [53]). In this case, we get suppression without oscillations for scales of interest.

The other model of interest is the decay of a charged particle into a CDM particle after BBN [40]. In this model, the initial conditions for the CDM perturbations are derived from the tightly

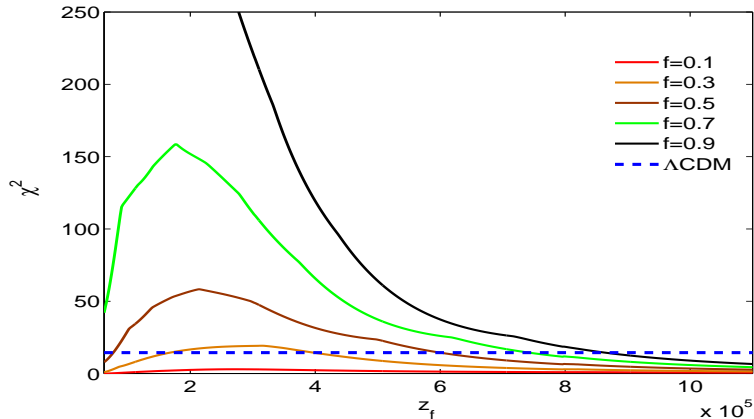


**Figure 6.**  $\chi^2$  is plotted as a function of  $z_f$  for many different values of  $f_{\text{fdm}}$  for the Lyman- $\alpha$  data. The dotted horizontal line is the  $\chi^2$  for the  $\Lambda$ CDM model.

coupled photon-Baryon Plasma. We compute the impact of of this process on the resultant power spectrum by assuming the decay to be a sharp transition. We compare the matter power spectrum in this case with the LFDM model in Figure 8 for the same formation redshift in both cases. As noted above, the initial conditions for the LFDM model come from massless neutrinos (Figure 1). The impact of the difference of initial conditions in the two cases can clearly be seen in Figure 8: for LFDM model neutrino oscillations follow an exponential slope below the scale of the horizon entry at the formation redshift. However, for the charged decay particle, the photon-baryon plasma oscillate inside the horizon with characteristic scales determined by the sound velocity of the coupled photon-baryon fluid and its decay scale is determined by Silk damping (for details see Figure 3 of [54] and the discussion preceding it).

## 6 Discussion

In this work we have investigated the epoch of dark matter formation in the universe for a class of non-standard (non-WIMP) dark matter scenarios. Especially we have studied how late the dark matter can form. Unlike the case of electroweak WIMP where dark matter formation happens through thermal freeze-out at a temp  $T \simeq \text{GeV}$ , in our models the dark matter formation happens considerably after BBN but before the CMBR decoupling. Our study is mainly inspired by a few viable models of "late forming dark matter" [35, 40]. In such models the matter power is suppressed at small scales which can be probed by cosmological observables at low redshifts using the available data on the linear power spectrum.

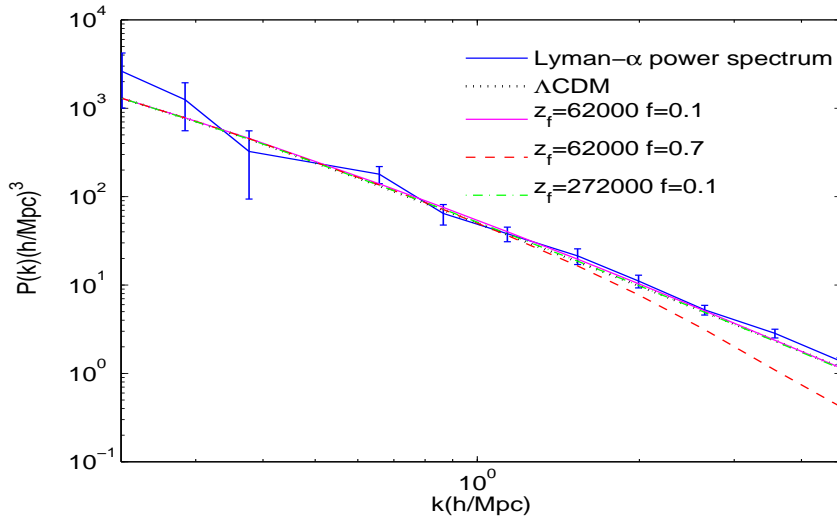


**Figure 7.** The band-powers corresponding to linear matter power spectrum extracted from Lyman- $\alpha$  data are shown [59, 61]. Also shown are the  $\Lambda$ CDM model and three LFDm models for a range of  $z_f$  and  $f_{\text{ifdm}}$ .

In the present study we confront models of LFDm with the existing SDSS data on galaxy power spectrum and the linear power spectrum extracted from Lyman- $\alpha$  data for  $z > 2$ . Our results can be summarized as follows: (a) if all the presently observed CDM is late forming then both the data sets result in upper limits on the redshift of formation of LFDm, with Lyman- $\alpha$  data resulting in tighter bounds:  $z_f < 3 \times 10^6$  (99% confidence limit) (Figure 3), (b) if we allow only a fraction of the CDM to form at late times, then we improve the quality of fit as compared to the  $\Lambda$ CDM model for the Lyman- $\alpha$  data. This is suggestive that the present data allows for a fraction of the CDM to form at  $z_f \simeq 10^5$  (Figure 5). In particular our result underlines the importance of the Lyman- $\alpha$  data for our study. In the recent past, the quantity of Lyman- $\alpha$  data available has sharply increased with the ongoing survey SDSS-III/BOSS [65]; and the results from this survey are expected to throw further light on the models of LFDm. We hope to return to this issue with as the new data becomes available.

We compare the predictions of our model with a few well-studied models that also result in a suppression of matter power at small scales (Figure 8). Different models—LFDm, charged decay model, and WDM—result in varying scales of characteristic oscillations and decay. The upcoming data might enable one to distinguish between these different deviations from the standard  $\Lambda$ CDM model and we hope to return to this issue in the near future.

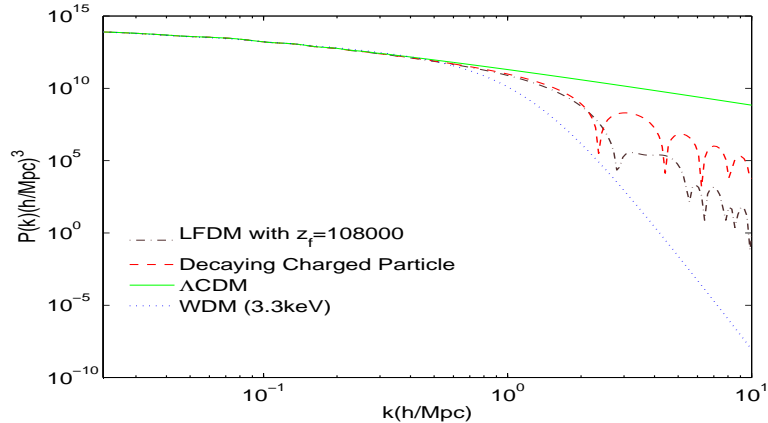


**Figure 8.** The LFDM results are compared to other models that also predict suppression of matter power at small scales. The power spectra (unnormalized) for WDM and the charged decay models follow from [29] and [40], respectively. In the charged decay model, the decay redshift is the same as the formation redshift for the LFDM model shown in the Figure.

Another possible future direction involves doing detailed N-body simulation of this model to see if there is any specific signatures of LFDM at small scale non-linear structure formation. Another interesting study could be the effect of LFDM on the epoch of the formation of first stars. Both of these studies are beyond the scope of this paper and have been kept for the future work.

## 7 Acknowledgment

We would like to thank Anze Slosar for his useful suggestions and comments and also to Daniel Boriero for the help with the SDSS power spectrum data. We thank Pier Stefano Corasaniti for sending useful comments.

## References

- [1] **Planck** Collaboration, P. Ade et al., *Planck 2013 results. XVI. Cosmological parameters*, *Astron.Astrophys.* (2014) [[arXiv:1303.5076](#)].
- [2] **WMAP** Collaboration, G. Hinshaw et al., *Nine-Year Wilkinson Microwave Anisotropy Probe (WMAP) Observations: Cosmological Parameter Results*, *Astrophys.J.Suppl.* **208** (2013) 19, [[arXiv:1212.5226](#)].
- [3] **Atacama Cosmology Telescope** Collaboration, J. L. Sievers et al., *The Atacama Cosmology Telescope: Cosmological parameters from three seasons of data*, *JCAP* **1310** (2013) 060, [[arXiv:1301.0824](#)].

- [4] M. Bartelmann and P. Schneider, *Weak gravitational lensing*, *Phys.Rept.* **340** (2001) 291–472, [[astro-ph/9912508](#)].
- [5] K. Begeman, A. Broeils, and R. Sanders, *Extended rotation curves of spiral galaxies: Dark haloes and modified dynamics*, *Mon.Not.Roy.Astron.Soc.* **249** (1991) 523.
- [6] B. Benson, T. de Haan, J. Dudley, C. Reichardt, K. Aird, et al., *Cosmological Constraints from Sunyaev-Zel’dovich-Selected Clusters with X-ray Observations in the First 178 Square Degrees of the South Pole Telescope Survey*, *Astrophys.J.* **763** (2013) 147, [[arXiv:1112.5435](#)].
- [7] **SDSS Collaboration**, M. Tegmark et al., *Cosmological Constraints from the SDSS Luminous Red Galaxies*, *Phys.Rev.* **D74** (2006) 123507, [[astro-ph/0608632](#)].
- [8] **SDSS Collaboration**, M. Tegmark et al., *Cosmological parameters from SDSS and WMAP*, *Phys.Rev.* **D69** (2004) 103501, [[astro-ph/0310723](#)].
- [9] G. Angloher, M. Bauer, I. Bavykina, A. Bento, C. Bucci, et al., *Results from 730 kg days of the CRESST-II Dark Matter Search*, *Eur.Phys.J.* **C72** (2012) 1971, [[arXiv:1109.0702](#)].
- [10] **XENON100 Collaboration** Collaboration, E. Aprile et al., *First Dark Matter Results from the XENON100 Experiment*, *Phys.Rev.Lett.* **105** (2010) 131302, [[arXiv:1005.0380](#)].
- [11] **XENON100 Collaboration** Collaboration, E. Aprile et al., *Dark Matter Results from 225 Live Days of XENON100 Data*, *Phys.Rev.Lett.* **109** (2012) 181301, [[arXiv:1207.5988](#)].
- [12] **CDMS-II Collaboration** Collaboration, Z. Ahmed et al., *Results from a Low-Energy Analysis of the CDMS II Germanium Data*, *Phys.Rev.Lett.* **106** (2011) 131302, [[arXiv:1011.2482](#)].
- [13] **LUX Collaboration** Collaboration, D. Akerib et al., *First results from the LUX dark matter experiment at the Sanford Underground Research Facility*, *Phys.Rev.Lett.* **112** (2014) 091303, [[arXiv:1310.8214](#)].
- [14] **PAMELA Collaboration** Collaboration, O. Adriani et al., *An anomalous positron abundance in cosmic rays with energies 1.5-100 GeV*, *Nature* **458** (2009) 607–609, [[arXiv:0810.4995](#)].
- [15] **PAMELA Collaboration** Collaboration, O. Adriani et al., *PAMELA results on the cosmic-ray antiproton flux from 60 MeV to 180 GeV in kinetic energy*, *Phys.Rev.Lett.* **105** (2010) 121101, [[arXiv:1007.0821](#)].
- [16] O. Adriani, G. Barbarino, G. Bazilevskaia, R. Bellotti, M. Boezio, et al., *A new measurement of the antiproton-to-proton flux ratio up to 100 GeV in the cosmic radiation*, *Phys.Rev.Lett.* **102** (2009) 051101, [[arXiv:0810.4994](#)].
- [17] **PAMELA Collaboration** Collaboration, O. Adriani et al., *The cosmic-ray electron flux measured by the PAMELA experiment between 1 and 625 GeV*, *Phys.Rev.Lett.* **106** (2011) 201101, [[arXiv:1103.2880](#)].
- [18] **Fermi LAT Collaboration** Collaboration, M. Ackermann et al., *Measurement of separate cosmic-ray electron and positron spectra with the Fermi Large Area Telescope*, *Phys.Rev.Lett.* **108** (2012) 011103, [[arXiv:1109.0521](#)].
- [19] **Fermi LAT Collaboration** Collaboration, M. Ackermann et al., *Fermi LAT observations of cosmic-ray electrons from 7 GeV to 1 TeV*, *Phys.Rev.* **D82** (2010) 092004, [[arXiv:1008.3999](#)].
- [20] **Fermi LAT Collaboration** Collaboration, A. A. Abdo et al., *Measurement of the Cosmic Ray  $e^+$  plus  $e^-$  spectrum from 20 GeV to 1 TeV with the Fermi Large Area Telescope*, *Phys.Rev.Lett.* **102** (2009) 181101, [[arXiv:0905.0025](#)].
- [21] **HEAT Collaboration** Collaboration, S. Barwick et al., *Measurements of the cosmic ray positron fraction from 1-GeV to 50-GeV*, *Astrophys.J.* **482** (1997) L191–L194, [[astro-ph/9703192](#)].
- [22] **AMS-01 Collaboration** Collaboration, M. Aguilar et al., *Cosmic-ray positron fraction measurement from 1 to 30-GeV with AMS-01*, *Phys.Lett.* **B646** (2007) 145–154, [[astro-ph/0703154](#)].
- [23] J. Goodman, M. Ibe, A. Rajaraman, W. Shepherd, T. M. Tait, et al., *Constraints on Light Majorana dark Matter from Colliders*, *Phys.Lett.* **B695** (2011) 185–188, [[arXiv:1005.1286](#)].
- [24] P. J. Fox, R. Harnik, J. Kopp, and Y. Tsai, *Missing Energy Signatures of Dark Matter at the LHC*, *Phys.Rev.* **D85** (2012) 056011, [[arXiv:1109.4398](#)].

- [25] D. Hooper, *Revisiting XENON100's Constraints (and Signals?) For Low-Mass Dark Matter*, *JCAP* **1309** (2013) 035, [[arXiv:1306.1790](#)].
- [26] J. L. Feng, A. Rajaraman, and F. Takayama, *Superweakly interacting massive particles*, *Phys.Rev.Lett.* **91** (2003) 011302, [[hep-ph/0302215](#)].
- [27] A. Dolgov and S. Hansen, *Massive sterile neutrinos as warm dark matter*, *Astropart.Phys.* **16** (2002) 339–344, [[hep-ph/0009083](#)].
- [28] S. Das and K. Sigurdson, *Cosmological Limits on Hidden Sector Dark Matter*, *Phys.Rev.* **D85** (2012) 063510, [[arXiv:1012.4458](#)].
- [29] M. Viel, G. D. Becker, J. S. Bolton, and M. G. Haehnelt, *Warm dark matter as a solution to the small scale crisis: New constraints from high redshift Lyman- $\alpha$  forest data*, *Phys.Rev.* **D88** (2013) 043502, [[arXiv:1306.2314](#)].
- [30] S. Tremaine and J. Gunn, *Dynamical Role of Light Neutral Leptons in Cosmology*, *Phys.Rev.Lett.* **42** (1979) 407–410.
- [31] J. March-Russell, S. M. West, D. Cumberbatch, and D. Hooper, *Heavy Dark Matter Through the Higgs Portal*, *JHEP* **0807** (2008) 058, [[arXiv:0801.3440](#)].
- [32] B. Patt and F. Wilczek, *Higgs-field portal into hidden sectors*, [hep-ph/0605188](#).
- [33] A. Dias, A. Machado, C. Nishi, A. Ringwald, and P. Vaudrevange, *The Quest for an Intermediate-Scale Accidental Axion and Further ALPs*, *JHEP* **1406** (2014) 037, [[arXiv:1403.5760](#)].
- [34] K. S. Jeong, M. Kawasaki, and F. Takahashi, *Axions as Hot and Cold Dark Matter*, *JCAP* **1402** (2014) 046, [[arXiv:1310.1774](#)].
- [35] S. Das and N. Weiner, *Late Forming Dark Matter in Theories of Neutrino Dark Energy*, *Phys.Rev.* **D84** (2011) 123511, [[astro-ph/0611353](#)].
- [36] A. A. Klypin, A. V. Kravtsov, O. Valenzuela, and F. Prada, *Where are the missing Galactic satellites?*, *Astrophys.J.* **522** (1999) 82–92, [[astro-ph/9901240](#)].
- [37] B. Moore, S. Ghigna, F. Governato, G. Lake, T. R. Quinn, et al., *Dark matter substructure within galactic halos*, *Astrophys.J.* **524** (1999) L19–L22, [[astro-ph/9907411](#)].
- [38] S. Garrison-Kimmel, M. Boylan-Kolchin, J. S. Bullock, and E. N. Kirby, *Too Big to Fail in the Local Group*, [arXiv:1404.5313](#).
- [39] M. Boylan-Kolchin, J. S. Bullock, and M. Kaplinghat, *Too big to fail? The puzzling darkness of massive Milky Way subhaloes*, *Mon.Not.Roy.Astron.Soc.* **415** (2011) L40, [[arXiv:1103.0007](#)].
- [40] K. Sigurdson and M. Kamionkowski, *Charged - particle decay and suppression of small - scale power*, *Phys.Rev.Lett.* **92** (2004) 171302, [[astro-ph/0311486](#)].
- [41] S. Das, *Sterile neutrino, hidden dark matter and their cosmological signatures*, *J.Phys.Conf.Ser.* **405** (2012) 012011.
- [42] E. Di Valentino, A. Melchiorri, and O. Mena, *Dark Radiation candidates after Planck*, [arXiv:1304.5981](#).
- [43] M. Archidiacono, N. Fornengo, S. Gariazzo, C. Giunti, S. Hannestad, et al., *Light sterile neutrinos after BICEP-2*, *JCAP* **1406** (2014) 031, [[arXiv:1404.1794](#)].
- [44] B. Bozek, D. J. E. Marsh, J. Silk, and R. F. G. Wyse, *Galaxy UV-luminosity Function and Reionisation Constraints on Axion Dark Matter*, [arXiv:1409.3544](#).
- [45] D. J. Marsh, E. Macaulay, M. Trebitsch, and P. G. Ferreira, *Ultra-light Axions: Degeneracies with Massive Neutrinos and Forecasts for Future Cosmological Observations*, *Phys.Rev.* **D85** (2012) 103514, [[arXiv:1110.0502](#)].
- [46] R. Hlozek, D. Grin, D. J. E. Marsh, and P. G. Ferreira, *A search for ultra-light axions using precision cosmological data*, [arXiv:1410.2896](#).
- [47] R. J. Wilkinson, C. Boehm, and J. Lesgourgues, *Constraining Dark Matter-Neutrino Interactions using the CMB and Large-Scale Structure*, *JCAP* **1405** (2014) 011, [[arXiv:1401.7597](#)].

- [48] N. Afshordi, M. Zaldarriaga, and K. Kohri, *On the stability of dark energy with mass-varying neutrinos*, *Phys. Rev.* **D72** (2005) 065024, [[astro-ph/0506663](#)].
- [49] N. Brouzakis and N. Tetradis, *Static configurations of dark energy and dark matter*, *JCAP* **0601** (2006) 004, [[astro-ph/0509755](#)].
- [50] S. Das and K. Sigurdson, *Dark matter from micro nuggets of degenerate ultra light sterile fermions*, [work in progress](#).
- [51] V. Shvartsman, *Density of relict particles with zero rest mass in the universe*, *Pisma Zh.Eksp.Teor.Fiz.* **9** (1969) 315–317.
- [52] G. Mangano and P. D. Serpico, *A robust upper limit on  $N_{\text{eff}}$  from BBN, circa 2011*, *Phys.Lett.* **B701** (2011) 296–299, [[arXiv:1103.1261](#)].
- [53] J. Lesgourgues, G. Mangano, G. Miele, and S. Pastor, *Neutrino Cosmology*. Cambridge University Press, Cambridge U.K., 2013.
- [54] C.-P. Ma and E. Bertschinger, *Cosmological perturbation theory in the synchronous and conformal Newtonian gauges*, *Astrophys.J.* **455** (1995) 7–25, [[astro-ph/9506072](#)].
- [55] A. Lewis, A. Challinor, and A. Lasenby, *Efficient computation of CMB anisotropies in closed FRW models; CAMB Code Home Page, <http://camb.info>*, *Astrophys.J.* **538** (2000) 473–476, [[astro-ph/9911177](#)].
- [56] P. Peebles and J. Yu, *Primeval adiabatic perturbation in an expanding universe*, *Astrophys.J.* **162** (1970) 815–836.
- [57] B. A. Reid, W. J. Percival, D. J. Eisenstein, L. Verde, D. N. Spergel, et al., *Cosmological Constraints from the Clustering of the Sloan Digital Sky Survey DR7 Luminous Red Galaxies*, *Mon.Not.Roy.Astron.Soc.* **404** (2010) 60–85, [[arXiv:0907.1659](#)].
- [58] **Virgo Consortium** Collaboration, R. Smith et al., *Stable clustering, the halo model and nonlinear cosmological power spectra*, *Mon.Not.Roy.Astron.Soc.* **341** (2003) 1311, [[astro-ph/0207664](#)].
- [59] R. A. Croft, D. H. Weinberg, M. Bolte, S. Burles, L. Hernquist, et al., *Towards a precise measurement of matter clustering: Lyman alpha forest data at redshifts 2–4*, *Astrophys.J.* **581** (2002) 20–52, [[astro-ph/0012324](#)].
- [60] N. Y. Gnedin and A. J. Hamilton, *Matter power spectrum from the Lyman-alpha forest: Myth or reality?*, *Mon.Not.Roy.Astron.Soc.* **334** (2002) 107–116, [[astro-ph/0111194](#)].
- [61] M. Tegmark and M. Zaldarriaga, *Separating the early universe from the late universe: Cosmological parameter estimation beyond the black box*, *Phys.Rev.* **D66** (2002) 103508, [[astro-ph/0207047](#)].
- [62] D. Parkinson, S. Riemer-Sorensen, C. Blake, G. B. Poole, T. M. Davis, et al., *The WiggleZ Dark Energy Survey: Final data release and cosmological results*, *Phys.Rev.* **D86** (2012) 103518, [[arXiv:1210.2130](#)].
- [63] C. Heymans, E. Grocutt, A. Heavens, M. Kilbinger, T. D. Kitching, et al., *CFHTLenS tomographic weak lensing cosmological parameter constraints: Mitigating the impact of intrinsic galaxy alignments*, *Mon.Not.Roy.Astron.Soc.* **432** (2013) 2433, [[arXiv:1303.1808](#)].
- [64] **SDSS Collaboration** Collaboration, P. McDonald et al., *The Linear theory power spectrum from the Lyman-alpha forest in the Sloan Digital Sky Survey*, *Astrophys.J.* **635** (2005) 761–783, [[astro-ph/0407377](#)].
- [65] N. Palanque-Delabrouille, C. Yèche, A. Borde, J.-M. L. Goff, G. Rossi, et al., *The one-dimensional Ly-alpha forest power spectrum from BOSS*, *Astron.Astrophys.* **559**, **A85** (2013) [[arXiv:1306.5896](#)].
- [66] K. L. Pandey and S. K. Sethi, *Probing Primordial Magnetic Fields Using Ly-alpha Clouds*, *Astrophys.J.* **762** (2013) 15, [[arXiv:1210.3298](#)].